Yamaguchi interferometer survey of protostellar outflows embedded in 70-µm dark infrared dark cloud

Keita Kitaguchi , Kazuhito Motogi , Kenta Fujisawa , Kotaro Niinuma , Ryotaro Fujiwara

YAMAGUCHI UNIVERSITY
山口大学

Introduction

1. High-mass star formation

- A number of evolved accretion disks in high-mass protostellar phase (e.g., Motogi et al. 2019, Maud et al. 2019, etc) has been found in the last decade, indicating that high-mass stars are formed by disk mediated accretion similar to that of lower mass stars.
  - ➢ **Star formation efficiency (M_{star}/M_{core}) is up to 50% below core scale [3] .**
- Typical mass of high-mass starless cores is 10-30 $M_{\odot}$. This is too small to form O-type stars implying additional accretion from natal clamps and/or filaments (e.g., Kong et al.2021).
  → "Global collapse" model [4] may be more universal than pure "massive core collapse" model [5].
  - ➢ How massive initial virialized core can become depends on pre-collapse condition of natal massive clump (e.g., temperature, density, and virial parameter, etc).
  - ➢ **It is essential to study a practical environment of natal clump and core just before gravitational collapse for quantitatively understanding high-mass star formation.**
- "Proto-high-mass protostars" (PHPs), which are still in low--intermediate mass stage but with high accretion rate, are possible seeds of a high-mass protostar. They are extremely young and still hold initial environment without significant feedback.
  - ➢ A lifetime of PHPs should be only 10^4 yr or less. They are statistically rare and still observationally unidentified.

2. IRDC : Infrared dark cloud

- Cold and dense high-mass clumps in the IRDC are precursors of high-mass star cluster (e.g., Rathborne et al. 2006, Peretto & Fuller 2010)
- 70-μm dark IRDC clumps (Figure 1) are mostly starless and considered to be the earliest stage of high-mass star formation.
- Recent ALMA observations detected protostellar outflows in such 70-μm dark IRDCs (e.g., Feng et al. 2016 ; Pillai et al.2019).
  → These outflow sources are the best candidates of PHP.

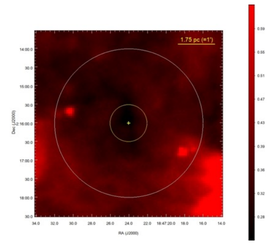

Fig1. Herschel 70μm image of IRDC G30.455-00.138.
○:YI's field of view
○: YI's spatial resolution

➢ High-mass protostellar jet/outflow are known to cause shock-driven free-free emission (e.g., Anglada et al. 2018) → So called 'radio jet'

We launched a new survey for free-free emission associated with such deeply embedded outflow shocks using the Yamaguchi Interferometer (YI: Fujisawa et al. 2022) at 8 GHz. We aim to compile a catalog of PHP candidates in 70-μm dark clumps . In this report, we present our preliminary results during Jan. 2020 and Jul. 2022.

Observation

Table 1 shows our observation parameters. Total 23 observations were made by YI from 1/10/2020 to 7/16/2022. The integration time was 1800 s for each target, 60 s for the flux calibrator (NRAO530, G33.50+0.20), and 300 s for the gain calibrator (J1919+0619).

Target selection criteria

Target sources are selected from "The initial conditions of stellar protocluster formation-II. A catalogue" (Traficante et al.2015), with following criteria.

1. $15° \leq l \leq 55°, 1° \leq |b|$ (l:galactic longitude, b:galactic latitude)
2. Starless-like clumps without any 70-μm point source.
3. Clumps with no nearby HII region in the YI's field of view.

< Data analysis >

We used the software correlator GICO3 developed by NICT for correlation processing and fringe search. Flux densities of the targets were relatively determined with respect to the known flux calibrators.

Table1. Observation parameters

YI (Yamaguchi 34 m, 32 m)	
Baseline	110 m
Frequency	8192-8704 MHz
Polarization	LHCP
Spatial resolution	1′.1
Field of view	4′.0
Integration time	1800 sec
Detection criterion	SNR > 7 σ
baseline sensitivity 1 σ	～ 0.5 mJy

Fig2. Yamaguchi Interferometer
(left)Yamaguchi 34 m
(right)Yamaguchi 32 m

Table2. Calibration objects

IAU name		RA(J2000)	Dec(J2000)	Application
J1733-1304	(Quasar)	17h32m02.7058s	-13d04'49".5482	Flux-calibration
G33.50+0.20	(HII region)	18h51m46.1789s	+00d35'32".3242	Flux-calibration
J1919+0619	(Quasar)	19h19m17.3504s	+06d19'42".7754	Gain-calibration

Results &Discussion

We detected 81 fringes from 167 clumps.

No CORNISH [12] counterpart were reported for detected radio sources.

- **Faint sources(< 20 mJy): 37 objects**

Figure 2 shows a histogram of target flux densities. Since flux densities of protostellar radio jets are typically fainter than 10 mJy, we conservatively defined a target below 20 mJy as a faint source (1.9 – 19.7 mJy) that can include young outflow shocks.

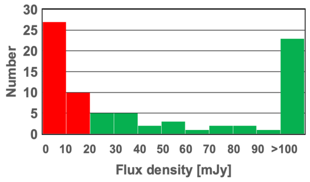

Fig2. Distributions of the flux density

- Bright source (≧ 20 mJy): 44 objects

They are too bright and likely to be background AGNs or unknown HII regions. The latter should be also background or deeply embedded because the targeted clumps are all 70-μm dark.

1. Characteristics of host IRDC clumps

Figure 3 shows a comparison of host clumps between the faint sources and other targets (non-detection sources and bright sources ≧ 20 mJy), where we compared surface densities of H_2 and dust temperatures. We found that the faint sources tend to associate with relatively colder and higher surface density clumps, i.e., suitable condition for star formation.

➢ **This fact suggests that some of them do trace star-formation actives such as young, deeply embedded outflow shock → They include possible PHP candidates !**

2. Surrounding environment of the faint sources

Next, we searched for evidences of star-formation activity for the 37 faint sources. We inspected whether cataloged masers and/or molecular outflows (e.g., [13]) exist within a host clump (～1 pc) or not. We found that 7 clumps were associated with masers and/or molecular outflows, 14 clumps were only detected by YI, and there were no maser or outflow observation for other 16 clumps. The 7 star-forming clumps have the highest surface densities at each temperature (see Figure 4).

➢ **A surface density at clump scale (～1 pc) seems to be closely associated with star-formation activity and it can be a good indicator of star-formation capability.**

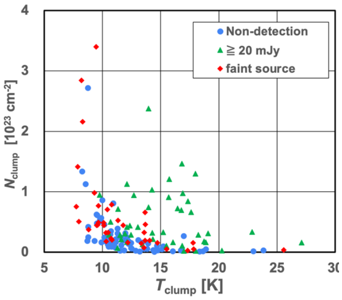

Fig3. Dust temperature vs. gas surface density for all the targets

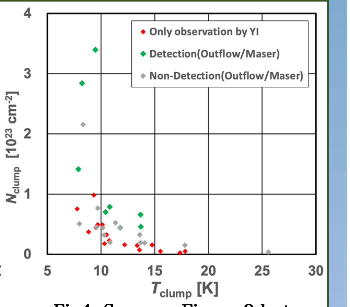

Fig4. Same as Figure 3 but only for the faint sources

3. Possible evolutionary phases of faint sources based on surrounding environments

The surrounding environments of the faint sources were categorized as shown in Table 5. These categories indicate that evolutionary difference already exist at 70-μm dark phase. We expect that evolution of the host clumps proceeds in the order of 1, 2, and 3. We will observe inversion transitions of NH_3 to study more detailed evolutionary stages.

Table5. Categories of surrounding environment of faint sources

category	Signs of star formation	Counts
1	Only radio source detected by YI	14
2	Outflow and/or maser within the clump	4
3	Signature of cluster formation around the clumps	4
Uncategorized	No other observation	15

Summary

- We are promoting new YI survey of protostellar outflow shocks deeply embedded in 70−μm IRDCs and 37 potential outflow candidates have already been detected.
- These faint sources tend associate with relatively colder and higher surface density clumps that are suitable for star formation.
- We investigated star formation activities of the host clumps and found that 7 clumps already associated with masers or molecular outflows. Furthermore, we identified the signature of cluster formation around 4 clumps suggesting that evolutionary difference already existed at 70−μm dark phase.

Reference

[1] Motogi, K., et al. 2019, ApJL 877,L25
[2] Maud, L.T., et al.2019, A&A, 627,L6
[3] Machida, M. N., & Hosokawa, T. 2013, mnras, 431, 1719
[4] Peretto, N., et al.2013, A&A, 555, A112
[5] Torii, K., et al.2017, ApJ, 835,142
[6] Kong, S., et al.2021, ApJ, 912,156
[7] Rathborne, J.M., et al. 2006, ApJL, 653,1325
[8] Peretto, N & Fuller, G.A., 2010 Apj, 723;555,562
[9] Feng, S., et al. 2016, ApJ, 883,202
[10] Pillai, T., et al.2019, A&A, 662,A59
[11] Fujisawa, K., et al.2022, PASJ, 74, 1415.
[12] CORNISH・https://cornish.leeds.ac.uk/public/cone.php
[13] MaserDB.net・ https://maserdb.net